Slow Carrier Cooling in Hybrid Pb-Sn Halide Perovskites

Sachin Dev Verma[1], **Qifei Gu**[1], **Aditya Sadhanala**[1,2], **Vijay Venugopalan**[1], **and Akshay Rao***,[1]

[1]Cavendish Laboratory, Department of Physics, University of Cambridge, JJ Thomson Avenue, Cambridge CB3 0HE, UK
[2]Clarendon Laboratory, Department of Physics, University of Oxford, Parks Road, Oxford OX1 3PU, UK

ABSTRACT: Low bandgap perovskites, such as mixed Pb-Sn systems, are essential to make bottom cells in all perovskite tandem photovoltaics. However, currently the fundamental dynamics of carriers in these materials are not well explored. Here we use ultrafast broadband pump-probe spectroscopy to probe the two-stage carrier cooling dynamics in $CH_3NH_3Pb_{1-x}Sn_xI_3$ perovskites and show that the cooling is slower than in pure Pb systems. The first stage of cooling is associated with Fröhlich interactions between carriers and metal-iodide bonds that slows down monotonically with increasing Sn content. The second stage of cooling involves the decay of optical phonon into acoustic phonons and is slowest for 60% Sn content, due to an increasing gap between the optical and acoustic phonon branches. Our results provide first insights into carrier cooling dynamics in hybrid Pb-Sn halide perovskites and pave the way for further understanding of the fundamental nature of Fröhlich interactions and the decay of optical phonons in perovskite systems.

TOC Graphic

1
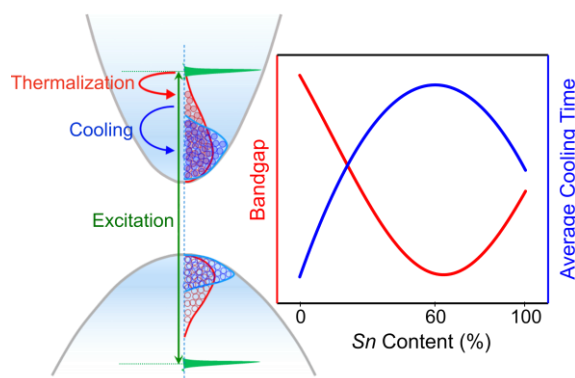
The unprecedented rise in power conversion efficiency (PCE) of lead-halide perovskites photovoltaics (PV) has established them as an excellent class of light-harvesting materials.[1] Facile solution processing and low processing cost make them ideal for contemporary solar energy research.[2] Intensive research has been devoted to single junction devices, where theoretical PCE of perovskite solar cell (SC) is restricted by Shockley-Queisser limit.[3] Recently, attention has focused on all perovskite tandem PV configurations which require a higher band gap (1.9-1.7 eV) top cell and a lower band gap (1.3-1.2 eV) bottom cell.[4–7] This necessitates the development and photophysical characterisation of low bandgap perovskites. Methylammonium lead-tin iodide ($CH_3NH_3Pb_{1-x}Sn_xI_3$) hybrid perovskites have paved the way to tune the band gap as low as 1.2 eV.[8] Photovoltaic devices based on these lead-tin mixed perovskites have been fabricated and shown to have encouraging device characteristics.[5] However, in contrast to the more widely explored Methylammonium lead iodide ($CH_3NH_3PbI_3$) systems, little is currently known about the ultrafast photophysics of these systems and how they affect device performance.

Optical excitation of semiconductors generates charge carriers. Carrier excitation with excess energy i.e. excitation energy higher than the band gap, produces a nonequilibrium distribution of carriers. Subsequently, carriers undergo carrier-carrier scattering which results in a quasi-equilibrium distribution of hot carrier having carrier temperature (T_C), higher than the lattice temperature (T_L). These hot carriers then go through carrier-optical-phonon scattering and cool down to the band extrema by dissipating their excess energy as heat to the lattice via phonon emission.[9] This whole cooling process is a major loss channel in photovoltaics, and partly contributes to the Shockley-Queisser limit. Understanding carrier thermalization provides not only fundamental insights into material properties but also paves the way for optimised charge extraction process. Thermalization and carrier cooling in inorganic semiconductors have been extensively studied using pump-probe and photoluminescence spectroscopies.[10–13] In hybrid perovskites, these studies[14–19] have found cooling on sub-picosecond timescale or faster. The ability to tune the rate of carrier cooling would thus be of both fundamental and technological interest.

In this letter, we present a systematic study on carrier cooling dynamics in methylammonium lead-tin iodide ($CH_3NH_3Pb_{1-x}Sn_xI_3$) perovskites by employing ultrafast broadband pump-probe spectroscopy, while tuning the stoichiometric ratio of Pb and Sn. The high energy tail of pump-probe spectra are analysed by means of Boltzmann distribution and carrier temperatures are calculated. Our results show an increase in carrier temperature and slower cooling dynamics upon Sn addition. We speculate that observed change in carrier temperatures and cooling dynamics are associated to the differences in the band structure and lattice parameters of $CH_3NH_3Pb_{1-x}Sn_xI_3$ perovskites. These findings provide first insights on carrier temperature and cooling dynamics in $CH_3NH_3Pb_{1-x}Sn_xI_3$ perovskites and how they can be controlled.

Thin films were prepared by spin-coating the precursor solution in desired stoichiometric ratios under N_2 atmosphere inside a glovebox (details in SI). Absorption spectra were measured using Photothermal deflection spectroscopy (PDS) (details in SI). Figure 1A displays linear
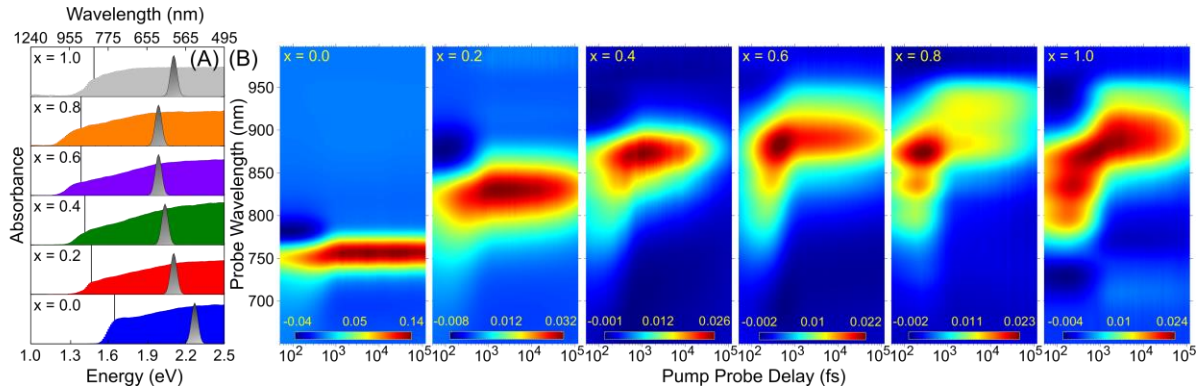
Figure 1. Linear absorption spectra of $CH_3NH_3Pb_{1-x}Sn_xI_3$, black vertical line is a guide to eye for the band gap and grey Gaussian spectra represent the pump energies used in pump-probe measurements for respective samples (A). Pump-probe maps of $CH_3NH_3Pb_{1-x}Sn_xI_3$ perovskites (B).

absorption spectra of $CH_3NH_3Pb_{1-x}Sn_xI_3$ for different Pb-Sn ratios. For $x = 0$ (pure Pb) the band edge is ~1.6eV which red shifts as Sn is added as a function of Sn content up to 60%. Subsequently, band edge blue shifts slightly for 80% and 100% Sn content. This bandgap bowing behaviour has been characterised in detail previously.[8,20,21] Black pulse in figure 1A represents the pump pulse energy. The pump pulse is tuned so as to provide the same excess energy above the bandgap within each material. Figure 1B shows pump-probe spectra of $CH_3NH_3Pb_{1-x}Sn_xI_3$ for different Sn content measured with the experimental setup described in SI.

All the pump-probe maps are composed of similar features, the main positive ground state bleach (GSB) band at 1.65, 1.5, 1.43, 1.4, 1.38, and 1.41 eV for 0, 20, 40, 60, 80, and 100% Sn content, respectively, accompanied by two negative photo-induced absorption (PIA) bands. The GSB band is attributed to band filling in semiconductors.[22] The PIA below the band gap is associated to band gap renormalization due to band gap shrinkage by photo-induced carriers.[14,15,22] A broad PIA is also observed at higher energies around 1.77, 1.75, 1.72, 1.70, 1.77, 1.70 eV for 0, 20, 40, 60, 80, and 100% Sn content, respectively. This higher energy PIA has earlier been assigned to photoinduced refractive index change in MAPI.[14] It can be clearly seen that the position of the GSB band shifts in accordance with the shift observed in the band gap. The GSB is broader for 20% Sn content and higher, and has a faster decay than that of pure Pb (figure S2 in SI). Differences in the GSB width can be associated with different band filling effects. Samples for all x are excited with energies such that carriers have same excess energy in respective bands. Excitation energy is centred around 2.26, 2.11, 2.04, 2.0, 2.0, and 2.11 for 0, 20, 40, 60, 80, and 100% Sn content, respectively (figure 1A). As noted above, these excitation energies provide the same excess energy of ~610 meV for the carriers in respective samples. The pump fluence is kept at 19 $\mu J/cm^2$ which is in linear regime (figure S1 in SI). Pump fluence is chosen to avoid multi-particle recombination and falls before the onset of hot phonon bottleneck effect.

Fits to the high energy tail of GSB band for the pure Pb sample are shown in figure 2A. The high energy tail of the pump-probe spectra are approximated with a Maxwell-Boltzmann distribution function and the carrier temperature is obtained directly from the fits. This is a standard method for calculating carrier temperature in semiconductors when employing both
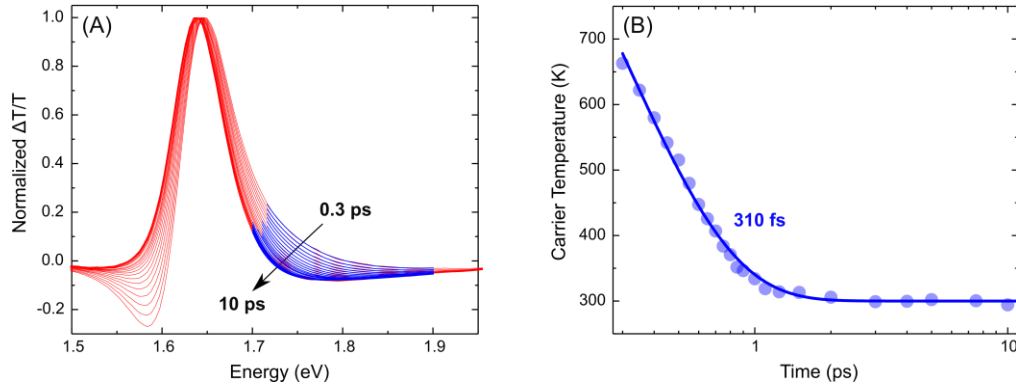
Figure 2. Normalized pump-probe spectra (red) of $CH_3NH_3PbI_3$ perovskite at different pump-probe delays (from 300 fs to 10 ps) fitted (blue) with Boltzmann distribution at high energy tail (A) and, calculated carrier temperatures (circles) fitted to a single exponential function (line) with decay constant of 310 fs(B).

pump-probe and transient photoluminescence spectroscopy.[10–13] Recently, this method has been applied to carrier cooling dynamics in different hybrid lead halide perovskite films, methylammonium lead bromide nanocrystals, and in 2D perovskites.[14–18,23] Carrier temperatures calculated from high energy tail fits of GSB band for pure Pb sample excited at pump fluence of 19 $\mu J/cm^2$ are show in figure 2B. The carrier cooling can be fitted by single exponential lifetime of 310 fs, in agreement with previous reports on this system.[14,15]

Carrier temperatures as a function of time for $CH_3NH_3Pb_{1-x}Sn_xI_3$ perovskites, for different Sn content, are calculated in similar fashion as for pure Pb. A comparison of cooling curves for all compositions is shown in figure 3A. Large changes in the initial carrier temperature are observed with changes in the Sn content and it is found that the initial temperature monotonically increases with increasing Sn content. Initial temperature depends on excess energy of the photo-induced carriers and the carrier density.[15] Note that all the samples are excited with same excess energy (~610 meV) and with same pump fluence (19 $\mu J/cm^2$), thus the differences in the initial temperature are unlikely to originate from a discrepancy in excess energy of the carriers or the pump fluence.

The increase in the initial temperatures upon increasing Sn content can be explained in terms of carrier-carrier-scattering. Exchange of energy among carriers is determined by carrier-carrier scattering and is mediated by Coulomb interaction. In hybrid perovskites, weaker Coulomb screening compared to semiconductors such as GaAs leads to faster carrier-carrier scattering. Addition of Sn to Pb based perovskites increases the effective dielectric constant and leads to stronger screening experienced by metal-halide lattice.[24] For a given carrier density stronger screening will give rise to slower carrier-carrier scattering time. Intrinsic carrier density increases upon decreasing the band gap, as is known for semiconductors such as Si and GaAs.[25] In Pb-Sn systems, the carrier density increases by three orders of magnitude with increasing Sn content from ~10^{11} for pure Pb sample to ~10^{14} for pure Sn sample.[8] Carrier-carrier scattering depends strongly on excess energy and carrier density.[26] For a given excess energy, a higher initial temperature due to higher carrier scattering rate at higher carrier densities is a commonly observed phenomenon in pervoskites.[14,15,26] Although the timescale of carrier-carrier scattering is faster than the time resolution (~250fs) of our experiments, the initial temperatures at the beginning of measured cooling curves are the end product of carrier-

4
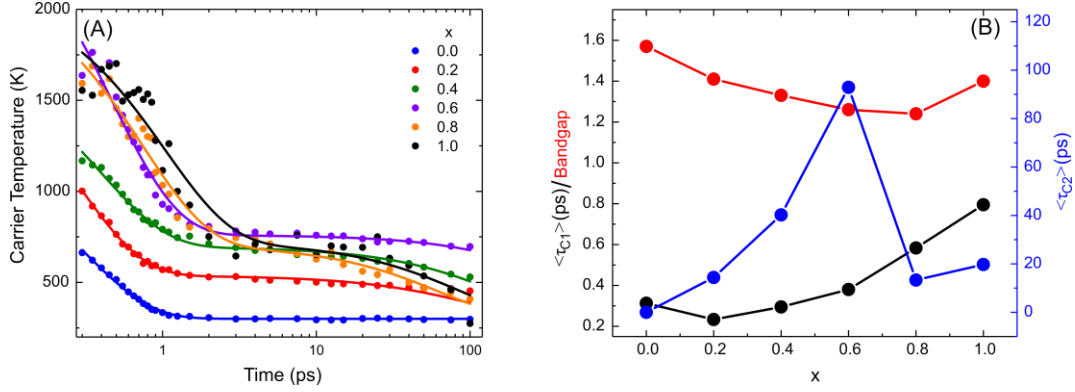
Figure 3. Carrier temperatures calculated from Boltzmann distribution fits to the high energy tails of CH$_3$NH$_3$Pb$_{1-x}$Sn$_x$I$_3$ perovskites (A). Average cooling time for first and second cooling stage calculated from biexponential fitting to the cooling curves (B). In (B), left axis works for both average cooling time for first stage (black) as well as bandgap (red).

carrier scattering. Therefore, we speculate that with increasing Sn content (decrease in bandgap) the increase in carrier density along with stronger screening leads to higher carrier scattering rate, which may give rise to a higher initial temperatures for the measured cooling curves.

The cooling curves obtained ranges from 300 fs to 100 ps. Two stage cooling is clearly visible for all Sn containing sample and can be modelled by two exponentials ($\sum_{i=1}^{2} a_i \exp(-t/\tau_i)$) with τ_i being the decay time. Average cooling time can be defined as $< \tau_{Ci} >= a_i \tau_i / \sum_{i=1}^{2} a_i$ where $i =1$ and 2 are for first, and second stage cooling, respectively. For pure Pb, where only one stage cooling is observed with decay time (τ_1) of ~310 fs, for 20% Sn containing sample τ_1 becomes slightly faster at ~275 fs. Further increase in Sn content shows monotonic increase in τ_1 as can be seen in the table 1. We do not wish to quantitatively comment on τ_1 for 80% and pure Sn containing sample due to noise. However, qualitatively it is clearly visible that they both have increasing trend. Therefore, on a qualitative level it is evident that for increasing Sn content there is a monotonic increase in τ_1. The average cooling time for first and second stages are shown in figure 3B and decay time constants are summarised in Table 1.

Table 1. Cooling curve fitting parameters and average cooling time. x is the fraction of Sn content, τ_1 and τ_2 are the decay constants of bi-exponential fitting to the cooling curves in figure 3A and correspond to first stage and second stage of cooling, respectively, weightage for decay constants are given in the brackets.

Sn content: x	decay time for first stage: τ_1 (fs)	decay time for second stage: τ_2 (ps)	avg. cooling time $< \tau >$ (ps)
0.0	310 (100)	0 (0)	0.3
0.2	275 (86)	100 (14)	15
0.4	400 (74)	150 (26)	41
0.6	470 (81)	500 (19)	93
0.8	740 (79)	60 (21)	14
1.0	1000 (77)	85 (23)	20

The first sub-picosecond stage of cooling in lead halide perovskites is associated with Fröhlich interactions between charge carriers and the lead-halide bond.[27,28] These interactions are important as charge carrier mobilities in semiconductors are fundamentally limited by these electron-phonon interactions.[29] The Fröhlich interaction is the main source of electron-phonon coupling near room temperature. In inorganic semiconductors, the electron-phonon coupling is mainly governed by two mechanisms, deformation potential scattering and piezoelectric/ electromechanical interactions.[29] In deformation potential scattering, the distortions of the lattice change the electronic band structure, and in piezoelectric/ electromechanical interactions, the electronic Hamiltonian is modified by lattice-related electric fields. Interaction between longitudinal optical (LO) phonons and electrons arises from the Coulomb interaction between the macroscopic electric field induced by the out-of-phase displacement of positively charged atoms caused by LO phonon modes and electrons.[29] Upon introducing Sn into MAPI, lattice distortion takes place and changes the band structure give rise to deformation potential scattering. Sn addition should also lead to increased effective dielectric constant giving rise to stronger screening resulting in suppressed rate of phonon emission.[24] In combination, deformation potential scattering and screened LO phonon-electron interaction give rise to observed differences in the first stage cooling dynamics upon increasing Sn content.

Interestingly, carriers do not cool down to lattice temperature within our experimental time window for all x > 0. There is no monotonic increase in the cooling time of the second stage with increasing Sn content as seen in first stage, however, the time constant for this stage is remarkably long compared to pure Pb sample. This cooling stage can be associate to the decay of LO phonon to low energy acoustic phonons.[10] As hot carriers relax to the bottom of the band a large number of LO phonons are emitted, these phonons primarily decay into two or more acoustic phonons. Thus, this second phase provides information on the optical phonon decay into acoustic phonons. This decay process depends on the phonon band gap between the optical branch and the acoustical branch. Cooling time can be controlled by modulating the phonon bandgap by mixing compounds with different atomic mass. Pb (207.2u) and Sn (118.71u) have very different atomic masses and thus can induce phonon bandgap tuning. Sn addition should also lead to elevated optical phonon frequencies of the lattice.[30] Phonon band gap opening by mixing the compounds having quite different atomic masses may lead to slow carrier cooling due to suppressed Klemens-decay mechanism.[31,32] For pure Pb sample, there is no second stage cooling. For the 20% Sn containing sample, the second cooling stage has τ_2 ~100 ps. This monotonically increases up to ~500 ps for 60% Sn containing sample (table 1). For 80% and pure Sn containing samples the trend is opposite, τ_2 becomes surprisingly fast (~60 ps) for the former and remains similar (~85 ps) for latter. We speculate that carrier recombination may be playing a role here as only decay of optical phonon to acoustic phonons alone can't explain the observed behaviour. This is supported by the fact that the GSB lifetime is relatively short for 80% and pure Sn containing samples (figure S2 in SI) and among them faster for 80% Sn content compared to pure Sn. Regardless, we see very slow cooling dynamics in Sn containing samples (figure 3B).

In summary, using broadband pump-probe spectroscopy we show that carrier cooling in methylammonium lead-tin iodide ($CH_3NH_3Pb_{1-x}Sn_xI_3$) perovskites is remarkably slow. Two

cooling stages are observed, and carriers do not reach the lattice temperature within our experimental time window of 100 ps. The first stage of cooling is associated with electron-phonon coupling through Fröhlich interactions, while the second stage of cooling is associated with the decay of optical phonon to acoustic phonons. The first stage gets faster upon introducing Sn (20%) and subsequently becomes slower with increasing Sn content. The second stage of cooling is not present for pure Pb sample and is much slower than the first stage of cooling for 20% Sn containing samples and continues to get slower with increasing Sn content up to 60%, after which it becomes much faster. For 60% Sn containing samples, the average cooling is slowest and the second cooling stage is more than two order of magnitude slower than first stage cooling. In comparison to average cooling time (~310 fs) of the pure Pb sample, samples with 60% Sn content have two order of magnitude slower average cooling time (~100 ps). Overall, our work presents a systematic study on carrier cooling dynamics in mixed Pb-Sn hybrid perovskites, and highlights that average cooling time can be slowed down by two order of magnitude. These measurements should spur further experimental and theoretical work to build a comprehensive understanding of electron-phonon interaction and decay of optical phonon to acoustic phonons in mixed Pb-Sn hybrid perovskite systems.

ASSOCIATED CONTENT

Supporting Information
The supporting information is available free of charge on the ACS Publication website at DOI: (link)

> Experimental methods, fluence dependent pump-probe signal, fluence dependence kinetics, fitting of high energy tail of pump-probe spectra (link).

AUTHOR INFORMATION

Corresponding Author
*Email: ar525@cam.ac.uk

ORCID
Sachin Dev Verma: 0000-0002-6312-9333
Aditya Sadhanala: 0000-0003-2832-4894
Vijay Venugopalan: 0000-0003-4701-5536
Akshay Rao: 0000-0003-4261-0766

Notes
The authors declare no competing financial interest.

ACKNOWLEDGEMENTS

REFERENCES

(1)   Correa-Baena, J.-P.; Abate, A.; Saliba, M.; Tress, W.; Jesper Jacobsson, T.; Grätzel, M.; Hagfeldt, A. The Rapid Evolution of Highly Efficient Perovskite Solar Cells. *Energy Environ. Sci.* **2017**, *10* (3), 710–727.

(2)   Snaith, H. J. Perovskites: The Emergence of a New Era for Low-Cost, High-Efficiency Solar Cells. *J. Phys. Chem. Lett.* **2013**, *4* (21), 3623–3630.

(3)   Shockley, W.; Queisser, H. J. Detailed Balance Limit of Efficiency of p-n Junction Solar Cells. *J. Appl. Phys.* **1961**, *32* (3), 510–519.

(4)   McMeekin, D. P.; Sadoughi, G.; Rehman, W.; Eperon, G. E.; Saliba, M.; Horantner, M. T.; Haghighirad, A.; Sakai, N.; Korte, L.; Rech, B.; et al. A Mixed-Cation Lead Mixed-Halide Perovskite Absorber for Tandem Solar Cells. *Science* **2016**, *351* (6269), 151–155.

(5)   Eperon, G. E.; Leijtens, T.; Bush, K. A.; Prasanna, R.; Green, T.; Wang, J. T.-W.; McMeekin, D. P.; Volonakis, G.; Milot, R. L.; May, R.; et al. Perovskite-Perovskite Tandem Photovoltaics with Optimized Band Gaps. *Science* **2016**, *354* (6314), 861–865.

(6)   Zhao, D.; Yu, Y.; Wang, C.; Liao, W.; Shrestha, N.; Grice, C. R.; Cimaroli, A. J.; Guan, L.; Ellingson, R. J.; Zhu, K.; et al. Low-Bandgap Mixed Tin–Lead Iodide Perovskite Absorbers with Long Carrier Lifetimes for All-Perovskite Tandem Solar Cells. *Nat. Energy* **2017**, *2* (4), 17018.

(7)   Meillaud, F.; Shah, A.; Droz, C.; Vallat-Sauvain, E.; Miazza, C. Efficiency Limits for Single-Junction and Tandem Solar Cells. *Sol. Energy Mater. Sol. Cells* **2006**, *90* (18–19), 2952–2959.

(8)   Hao, F.; Stoumpos, C. C.; Chang, R. P. H.; Kanatzidis, M. G. Anomalous Band Gap Behavior in Mixed Sn and Pb Perovskites Enables Broadening of Absorption Spectrum in Solar Cells. *J. Am. Chem. Soc.* **2014**, *136* (22), 8094–8099.

(9)   Shah, J. *Ultrafast Spectroscopy of Semiconductors and Semiconductor Nanostructures*; M. Cardona P. Fulde K. von Klitzing R. Merlin H.-J. Queisser H. Stormer, Ed.; Springer Series in Solid-State Sciences; Springer Berlin Heidelberg: Berlin, Heidelberg, 1999; Vol. 115.

(10)   Shah, J. Hot Electrons and Phonons under High Intensity Photoexcitation of Semiconductors. *Solid. State. Electron.* **1978**, *21* (1), 43–50.

(11)   Shank, C. V.; Fork, R. L.; Leheny, R. F.; Shah, J. Dynamics of Photoexcited GaAs Band-Edge Absorption with Subpicosecond Resolution. *Phys. Rev. Lett.* **1979**, *42* (2), 112–115.

(12)   Kash, K.; Shah, J. Carrier Energy Relaxation in $In_{0.53}Ga_{0.47}As$ Determined from Picosecond Luminescence Studies. *Appl. Phys. Lett.* **1984**, *45* (4), 401–403.

(13)   Lyon, S. A. Spectroscopy of Hot Carriers in Semiconductors. *J. Lumin.* **1986**, *35* (3), 121–154.

(14)   Price, M. B.; Butkus, J.; Jellicoe, T. C.; Sadhanala, A.; Briane, A.; Halpert, J. E.; Broch, K.; Hodgkiss, J. M.; Friend, R. H.; Deschler, F. Hot-Carrier Cooling and Photoinduced Refractive Index Changes in Organic–inorganic Lead Halide Perovskites. *Nat. Commun.* **2015**, *6* (1), 8420.

(15)   Yang, Y.; Ostrowski, D. P.; France, R. M.; Zhu, K.; van de Lagemaat, J.; Luther, J. M.; Beard, M. C. Observation of a Hot-Phonon Bottleneck in Lead-Iodide Perovskites. *Nat. Photonics* **2016**, *10* (1), 53–59.

(16)   Yang, J.; Wen, X.; Xia, H.; Sheng, R.; Ma, Q.; Kim, J.; Tapping, P.; Harada, T.; Kee, T. W.; Huang, F.; et al. Acoustic-Optical Phonon Up-conversion and Hot-Phonon Bottleneck

in Lead-Halide Perovskites. *Nat. Commun.* **2017**, *8* (1), 14120.

(17) Fu, J.; Xu, Q.; Han, G.; Wu, B.; Huan, C. H. A.; Leek, M. L.; Sum, T. C. Hot Carrier Cooling Mechanisms in Halide Perovskites. *Nat. Commun.* **2017**, *8* (1), 1300.

(18) Li, M.; Bhaumik, S.; Goh, T. W.; Kumar, M. S.; Yantara, N.; Grätzel, M.; Mhaisalkar, S.; Mathews, N.; Sum, T. C. Slow Cooling and Highly Efficient Extraction of Hot Carriers in Colloidal Perovskite Nanocrystals. *Nat. Commun.* **2017**, *8*, 14350.

(19) Fang, H.-H.; Adjokatse, S.; Shao, S.; Even, J.; Loi, M. A. Long-Lived Hot-Carrier Light Emission and Large Blue Shift in Formamidinium Tin Triiodide Perovskites. *Nat. Commun.* **2018**, *9* (1), 243.

(20) Im, J.; Stoumpos, C. C.; Jin, H.; Freeman, A. J.; Kanatzidis, M. G. Antagonism between Spin–Orbit Coupling and Steric Effects Causes Anomalous Band Gap Evolution in the Perovskite Photovoltaic Materials $CH_3NH_3Sn_{1-x}Pb_xI_3$. *J. Phys. Chem. Lett.* **2015**, *6*, 3503–3509.

(21) Zhao, B.; Abdi-Jalebi, M.; Tabachnyk, M.; Glass, H.; Kamboj, V. S.; Nie, W.; Pearson, A. J.; Puttisong, Y.; Gödel, K. C.; Beere, H. E.; et al. High Open-Circuit Voltages in Tin-Rich Low-Bandgap Perovskite-Based Planar Heterojunction Photovoltaics. *Adv. Mater.* **2017**, *29* (2), 1604744.

(22) Manser, J. S.; Kamat, P. V. Band Filling with Free Charge Carriers in Organometal Halide Perovskites. *Nat. Photonics* **2014**, *8* (9), 737–743.

(23) Jia, X.; Jiang, J.; Zhang, Y.; Qiu, J.; Wang, S.; Chen, Z.; Yuan, N.; Ding, J. Observation of Enhanced Hot Phonon Bottleneck Effect in 2D Perovskites. *Appl. Phys. Lett.* **2018**, *112* (14), 4–9.

(24) Umari, P.; Mosconi, E.; De Angelis, F. Infrared Dielectric Screening Determines the Low Exciton Binding Energy of Metal-Halide Perovskites. *J. Phys. Chem. Lett.* **2018**, *9* (3), 620–627.

(25) *Handbook Series on Semiconductor Parameters Volume 1*; M Levinshtein, S. R. and M. S., Ed.; World Scientific: London: London, 1996.

(26) Richter, J. M.; Branchi, F.; Valduga de Almeida Camargo, F.; Zhao, B.; Friend, R. H.; Cerullo, G.; Deschler, F. Ultrafast Carrier Thermalization in Lead Iodide Perovskite Probed with Two-Dimensional Electronic Spectroscopy. *Nat. Commun.* **2017**, *8* (1), 376.

(27) Wright, A. D.; Verdi, C.; Milot, R. L.; Eperon, G. E.; Pérez-Osorio, M. A.; Snaith, H. J.; Giustino, F.; Johnston, M. B.; Herz, L. M. Electron–Phonon Coupling in Hybrid Lead Halide Perovskites. *Nat. Commun.* **2016**, *7* (1), 11755.

(28) Kawai, H.; Giorgi, G.; Marini, A.; Yamashita, K. The Mechanism of Slow Hot-Hole Cooling in Lead-Iodide Perovskite: First-Principles Calculation on Carrier Lifetime from Electron–Phonon Interaction. *Nano Lett.* **2015**, *15* (5), 3103–3108.

(29) Yu, P. Y.; Cardona, M. *Fundamentals of Semiconductors*; Graduate Texts in Physics; Springer Berlin Heidelberg: Berlin, Heidelberg, 2010.

(30) Herz, L. M. How Lattice Dynamics Moderate the Electronic Properties of Metal-Halide Perovskites. *J. Phys. Chem. Lett.* **2018**, *9* (23), 6853–6863.

(31) König, D.; Casalenuovo, K.; Takeda, Y.; Conibeer, G.; Guillemoles, J. F.; Patterson, R.; Huang, L. M.; Green, M. A. Hot Carrier Solar Cells: Principles, Materials and Design. *Phys. E Low-dimensional Syst. Nanostructures* **2010**, *42* (10), 2862–2866.

(32) Conibeer, G. J.; König, D.; Green, M. A.; Guillemoles, J. F. Slowing of Carrier Cooling in Hot Carrier Solar Cells. *Thin Solid Films* **2008**, *516* (20), 6948–6953.